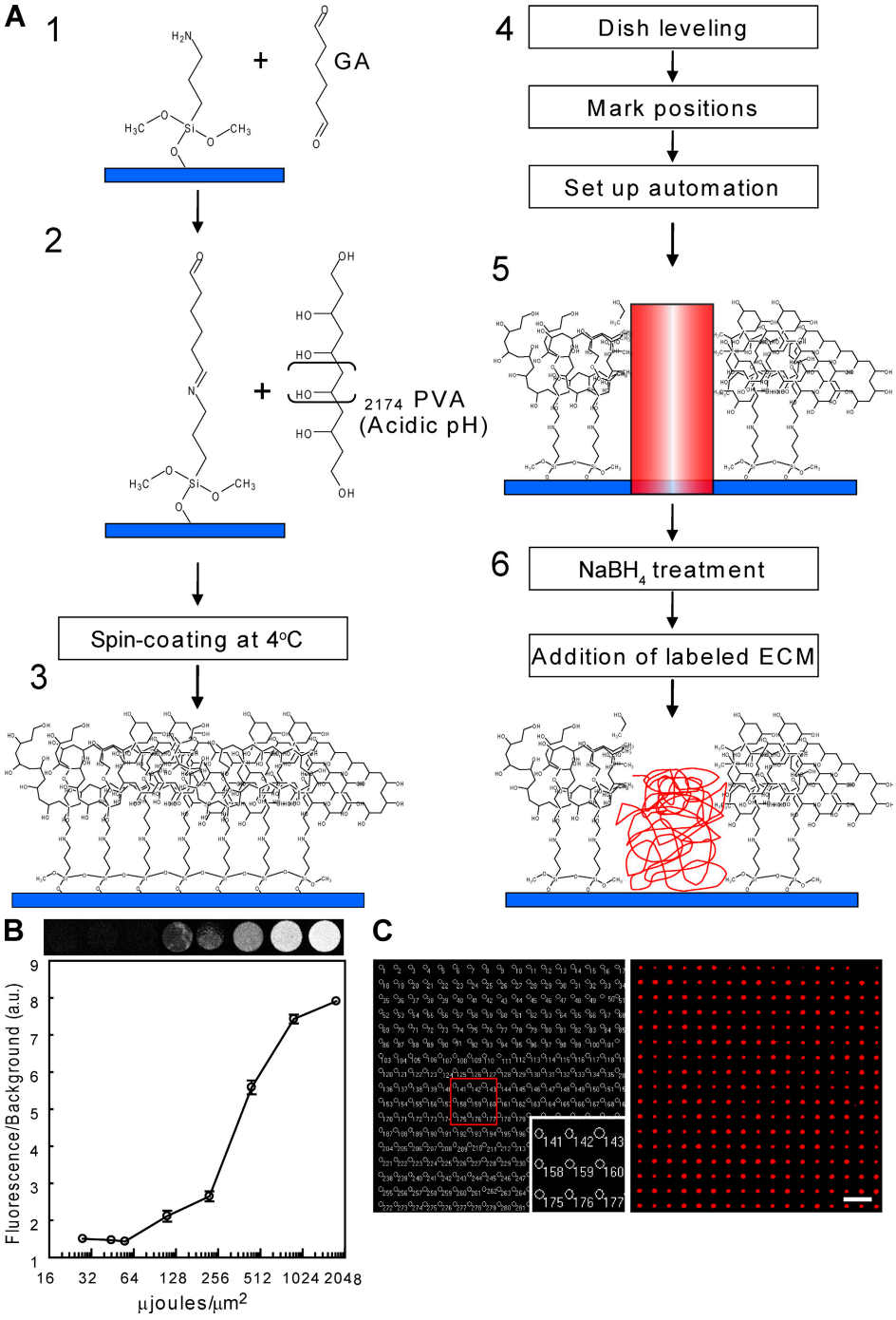

Figure S1. **Micropatterning with µPP.** (A) Process of µPP. (1) Acid-washed glass-bottom dishes or coverslips were silanized with 0.5% APTMS ((3-aminopropyl) trimethoxysilane), heat cured, and activated with 0.5% glutaraldehyde. (2) Activated surfaces were treated with an acidified 5% PVA solution and spin coated at 4°C, which forms a macromolecular thin film (3). (4) Before µPP, dishes are leveled throughout the field of view using stage set screws. Stage positions are marked to indicate ablation sites around which larger patterned arrays are centered using the tile function in the multitime automation macro. (5) PVA thin films were ablated using ~90% 755-nm excitation in the designated pattern. (6) 1 M $NaHB_4$ in 1 N NaOH was added to patterned dishes containing 200 mM ethanolamine in $NaHPO_3$ buffer, pH 8.0, at a 1:100 ratio for 8 min to quench glutaraldehyde autofluorescence. After treatment with $NaBH_4$, fluorescently labeled ECM proteins were added to the surface. (B) Efficiency of ECM protein adsorption to ablation sites is dependent on total light energy. Laser power was varied through the acoustooptic modulator and measured at the back focal plane of the objective to estimate joules per unit area. Total energy per unit area (µjoules/µm^2) was calculated from the measured wattage, and for the total dead time, the laser was focused on a given pixel area, which depended on scan speed and number of times scanned (line averaging function). (top) Representative fluorescence micrographs of AF568-labeled FN used for the graph below. (C) A representative ROI template (left) used to generate a dot-based pattern. Inset shows a magnification of the area represented by the red box. (right) AF647 FN conjugated to the ablation sites generated using the ROI template shown in A. Error bars indicate SEM. Bar, 10 µm.

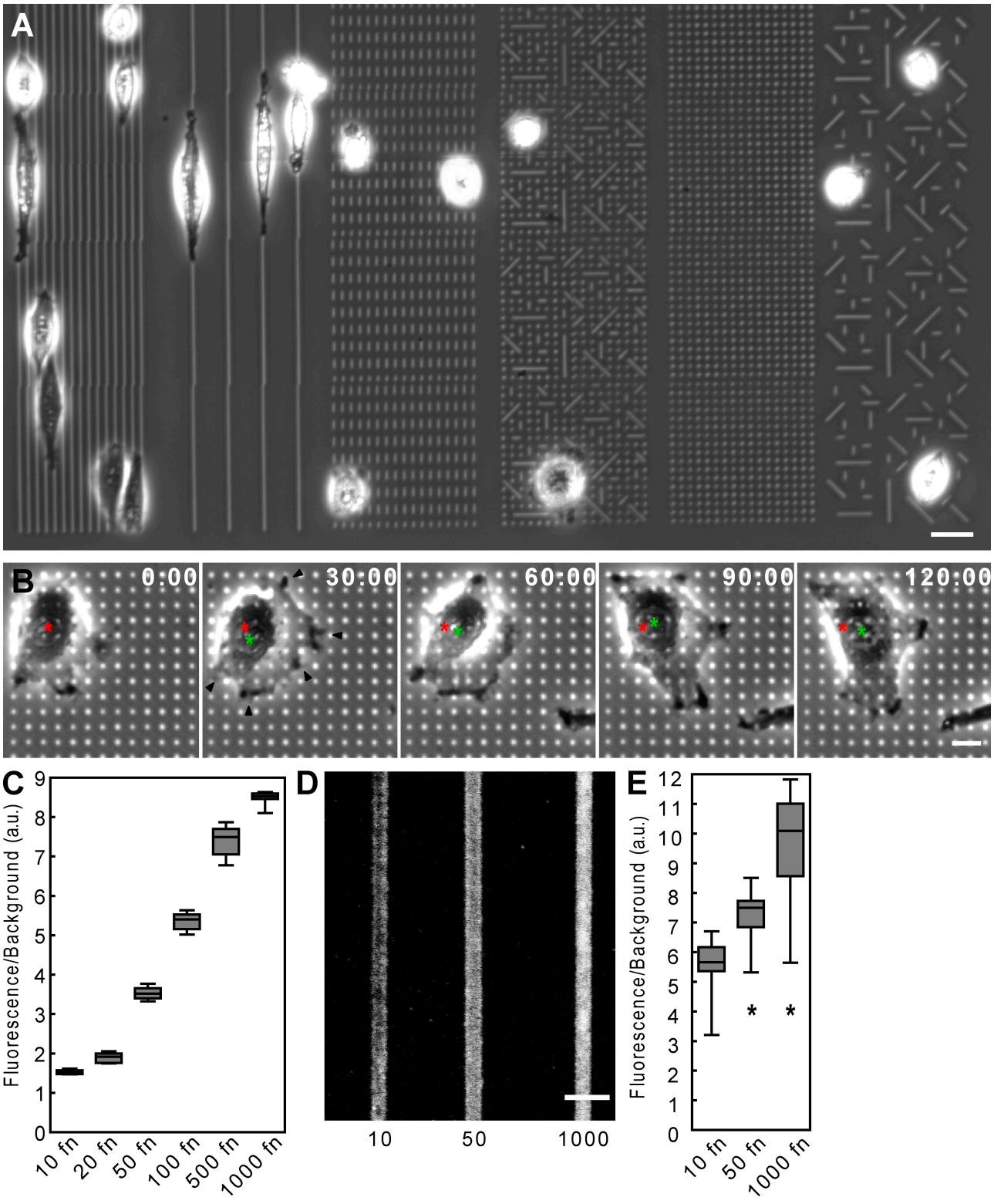

Figure S2. **Large-patterned arrays, dot patterns, and ECM ligand density data.** (A) A large-patterned array showing multiple patterns was used to determine how ECM topography dictates fibroblast migration. Bar, 20 µm. (B) Time-lapse images of a fibroblast moving slowly over a dot-based ECM pattern. Note the multiple sites of protrusive activity (black arrowheads) and the spread cell morphology. Red and green asterisks denote original and current nuclear position, respectively. Mean cell velocity was 8.26 µm/h. Bar, 10 µm. (C) Fluorescence of AF568-labeled FN on 2D culture dishes at varying concentrations after 1 h incubation at 37°C. (D) Fluorescence image of serial µPP in which 1,000, 50, and 10 µg/ml FN was adsorbed to the sequentially ablated lines. Bar, 5 µm. (E) Fluorescence of AF568-labeled FN on 1D µPP line patterns at 10, 50, and 1,000 µg/ml concentrations after 1 h incubation at 37°C. *, significant difference in fluorescence from 10 FN condition ($P < 0.05$). Error bars indicate SEM.

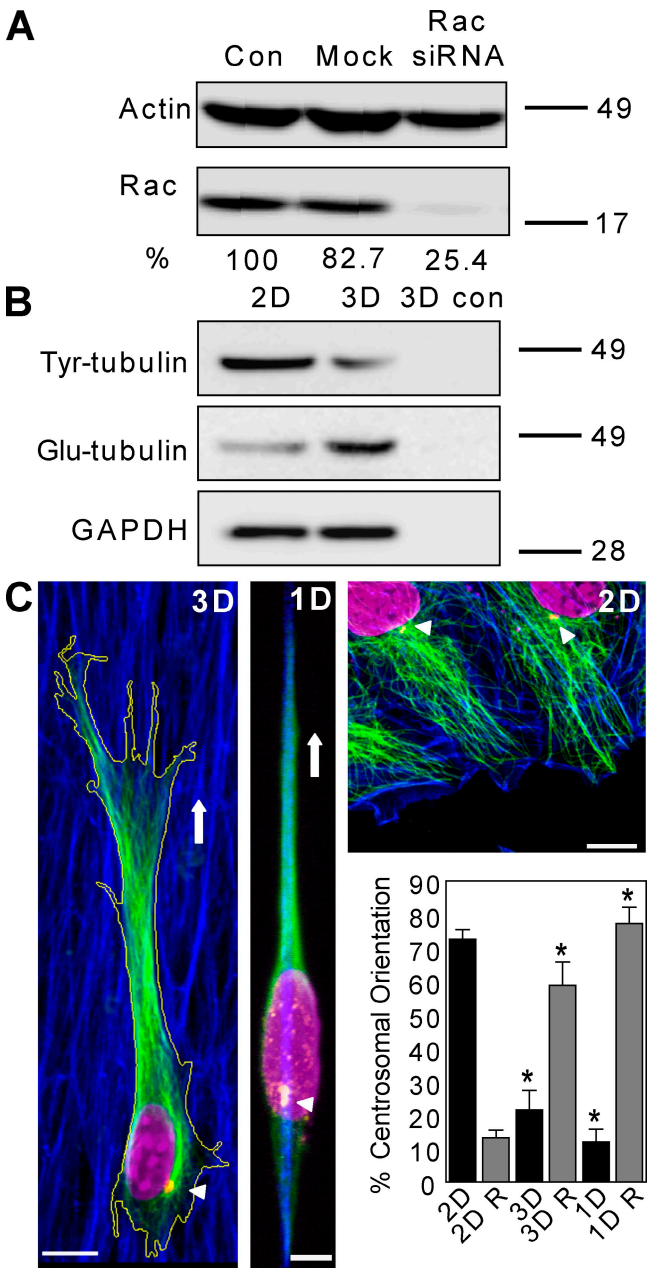

Figure S3. **Rac SiRNA, tubulin isoforms expression, and centrosome orientation data.** (A) Expression of actin and total Rac 72 h after transfection with control (Con) siRNA, mock transfection, and a single Rac siRNA duplex at 50 nM. Normalized expression level is shown below blots as a percentage. (B) Expression of tyrosinated (Tyr) tubulin, detyrosinated (Glu) tubulin, and glyceraldehyde 3-phosphate dehydrogenase (GAPDH) for 2D, and 3D cell-derived matrix with fibroblasts and 3D cell-derived matrix alone as a control. (C) Centrosome orientation in 1D and 3D environments is opposite to the classical frontal orientation found in 2D wound assays. The location of pericentrin (yellow) is indicated by arrowheads with respect to Tyr-tubulin (green) and the nucleus (purple). Blue indicates FN in 3D and 1D and actin in 2D. Arrows indicate the direction of migration. Bars: (1D and 2D) 5 µm; and (3D) 10 µm. *, significant difference from 2D wound assay control ($P < 0.05$). Error bars indicate SEM.

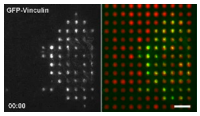

Video 1. **Focal adhesion formation during migration on dot-patterned substrates.** TIRF time-lapse imaging of NIH-3T3 fibroblasts expressing GFP-vinculin (left) migrating over dot micropatterns (~5 µm spacing). Overlay of GFP-vinculin (green) with DyLight 649–labeled 10 µg/ml FN dot micropatterns. Images were collected every 60 s and shown at 15 frames per second. Bar, 10 µm.

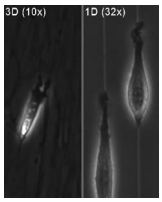

Video 2. **3D mimicry with 1D topography.** Side by side comparison of NIH-3T3 fibroblast migration through 3D cell-derived matrix (left) and over 1D fibrillar lines (right). Images were collected every 2 min and shown at 15 frames per second.

Video 3. **Multiple NIH-3T3 fibroblasts undergoing 1D fibrillar migration.** Images were collected every 4 min and shown at 15 frames per second.

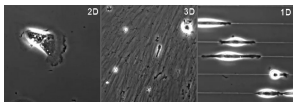

Video 4. **Topographical regulation of keratinocyte migration.** 2D, 3D, and 1D fibrillar migration of human epidermal keratinocytes. Images were collected every 4 min and shown at 15 frames per second.

Video 5. **1D fibrillar migration demonstrates unique adhesion assembly and disassembly patterns.** NIH-3T3 fibroblasts expressing GFP-vinculin undergoing adhesion assembly, anchorage, and disassembly during 1D fibrillar migration. Images were collected every 60 s and shown at 15 frames per second.

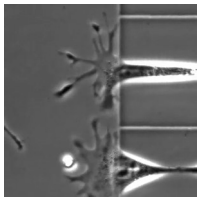

Video 6. **Transition from 1D to 2D migration: regulation of cellular phenotype by ECM topography.** Formation of multiaxial lamellae and cell spreading during the transition from 1D to 2D migration. Images were collected every 2 min and shown at 15 frames per second.

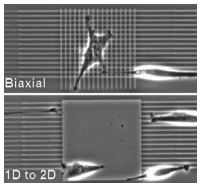

Video 7. **Off-axis patterns perturb uniaxial migration, whereas 1D lines promote conversion to fibrillar migration.** Effects of encountering a perpendicular fibrillar pattern during fibrillar migration (top) and conversion of 2D to 1D migration. Images were collected every 4 min and shown at 15 frames per second.